A COMPUTATIONAL MODEL FOR THREE-DIMENSIONAL INCOMPRESSIBLE WALL JETS WITH LARGE CROSS FLOW*

W.D. Murphy, V. Shankar, and N.D. Malmuth
Science Center
Rockwell International
Thousand Oaks, California 91360

SUMMARY

The flow field of three-dimensional incompressible wall jets prototypic of thrust augmenting ejectors with large cross flow is solved using a very efficient centered-Euler scheme in an orthogonal curvilinear coordinate system. The computational model treats initial conditions with arbitrary velocity profiles at the jet exit. An averaging approach is employed for the first few marching steps to overcome spurious numerical oscillations associated with arbitrary initial profiles. Laminar as well as turbulent wall jets are simulated. Turbulence is introduced using a two layer mixing length model appropriate to curved three-dimensional wall jets. Typical results quantifying jet spreading, jet growth, nominal separation and jet shrink effects due to cross flow are presented.

*This work was sponsored by the Naval Air Development Center under Contract N62269-77-C-0412. The monitor for this effort was Dr. Kenneth Green.

INTRODUCTION

Modern naval aircraft can reduce strike force vulnerability by the attainment of vertical lift-off capability. To achieve accelerations associated with typical payloads, a high augmentation ratio ϕ is required. Various propulsive lift concepts have been advanced toward obtaining this goal. In the XFV-12A, an ejector system composed of a centerbody and two Coanda wall jets is currently under development. A central feature of the flow fields produced by this device is three dimensionality. This has been particularly evident in subscale flow visualization on the Coanda surfaces. It is believed that these flow processes may be important toward ϕ maximization. One way of understanding this relationship is through theoretical modeling which can provide a means of reducing the high cost of powered lift testing. Unfortunately, existing methodology has been limited in the past to two-dimensional flows for the analysis of wall jets and complete ejector systems. Analytical methods and computational algorithms are therefore necessary to compute three-dimensional flows typical of reality.

To shed light on typical flow patterns encountered, due to the effect of taper and sweep on augmenter wings as well as upper-surface-blown configurations, a study, "Three-Dimensional Flow of a Wall Jet," was initiated by the Naval Air Development Center to investigate wall jet flows which exemplify typical features of more complex propulsive lift applications. The purpose of this study has been to apply modern computational methods to the treatment of wall jet flows with three dimensionality.

The formulation employs boundary-layer equations in an orthogonal curvilinear coordinate system. It can be shown from a systematic order of magnitude analysis that the boundary-layer equations also apply for wall jets, providing the distance from the jet exit is sufficiently large to establish complete mixing, the jet height is small compared to a characteristic radius of curvature, and the Reynolds number based on the exit height is large. A transformation is incorporated

to stretch the coordinate normal to the flow. At streamwise planes, the resulting nonlinear partial differential equations are treated as ordinary differential equations. These are solved using a very efficient two-point boundary value finite-difference method devised by Keller and Cebeci[1-3] known as "box method." The turbulence is introduced using a two-layer mixing length model appropriate to three-dimensional wall jets.

Equations in Curvilinear System

The governing equations for three-dimensional incompressible flows over a wall jet in a curvilinear orthogonal coordinate system shown in Figure 1 are given by the following equations:

Continuity

$$(\partial/\partial x)(h_2 u) + (\partial/\partial z)(h_1 w) + (\partial/\partial y)(h_1 h_2 v) = 0 \tag{1}$$

x-Momentum

$$\frac{u}{h_1}\frac{\partial u}{\partial x} + \frac{w}{h_2}\frac{\partial u}{\partial z} + v\frac{\partial u}{\partial y} - uwK_1 + w^2K_2 = -\frac{1}{\rho h_1}\frac{\partial p}{\partial x} + \frac{\partial}{\partial y}\left(\nu\frac{\partial u}{\partial y} - \overline{u'v'}\right) \tag{2}$$

z-Momentum

$$\frac{u}{h_1}\frac{\partial w}{\partial x} + \frac{w}{h_2}\frac{\partial w}{\partial z} + v\frac{\partial w}{\partial y} - uwK_2 + u^2K_1 = -\frac{1}{\rho h_2}\frac{\partial p}{\partial z} + \frac{\partial}{\partial y}\left(\nu\frac{\partial w}{\partial y} - \overline{w'v'}\right) \tag{3}$$

Here h_1 and h_2 are metric coefficients and are functions of x and z, and the parameters K_1 and K_2 are known as the geodesic curvatures of the curves z = const. and x = const., respectively.

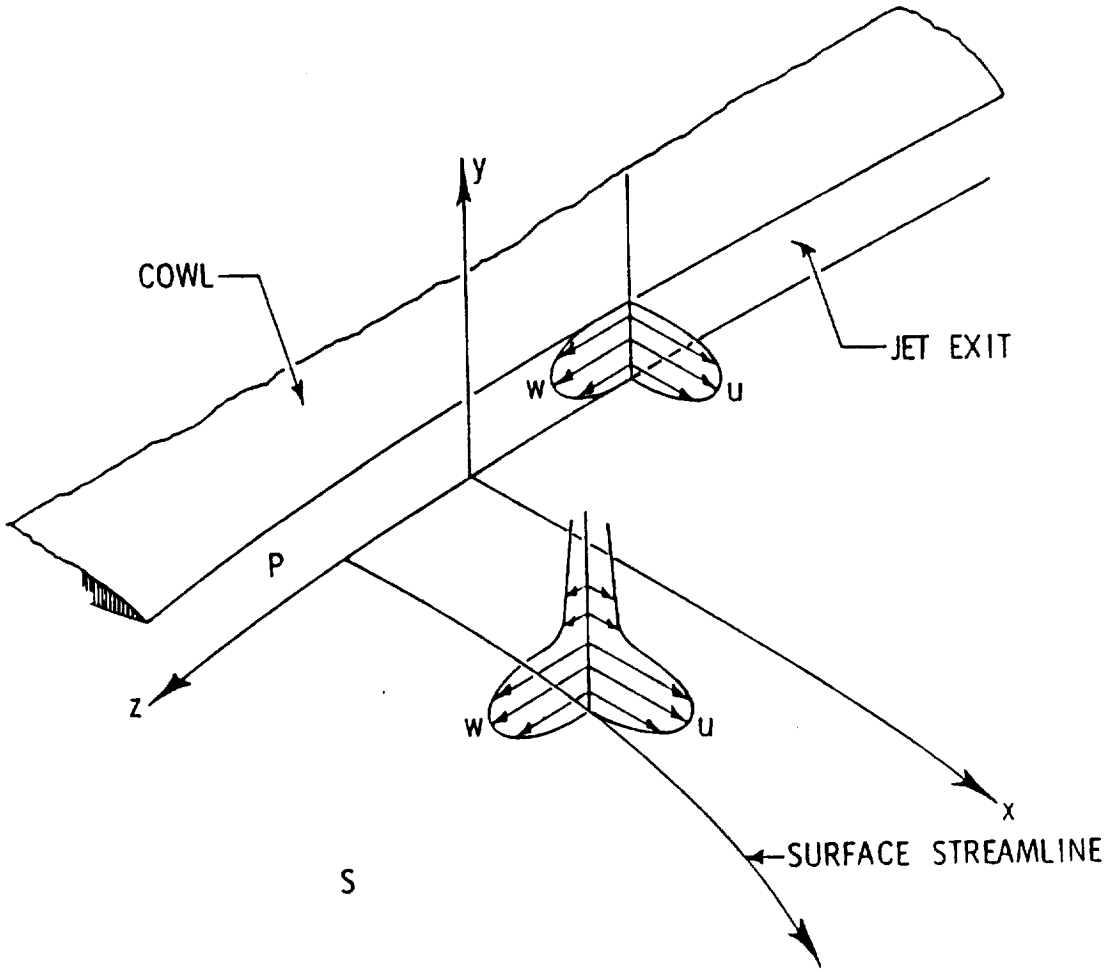

Figure 1.- Physical system and flow schematic.

The boundary conditions for Eqs. (1) through (3) for zero mass transfer are

$$y = 0 \qquad u,w,v = 0$$

$$y \to \infty \qquad u \to u_e(x,z) \qquad w \to w_e(x,z) \tag{4}$$

As indicated earlier, the previous equations are transformed by defining

$$x = x \qquad z = z \qquad \eta = (u_e/\nu s_1)^{\frac{1}{2}} y \tag{5}$$

and introducing a two-component vector potential given by

$$h_2 u = \frac{\partial \psi}{\partial y} \qquad h_1 w = \frac{\partial \phi}{\partial y} \qquad h_1 h_2 v = -\left(\frac{\partial \psi}{\partial x} + \frac{\partial \phi}{\partial z}\right) \tag{6}$$

In addition, the dimensionless variables f and g related to ψ and ϕ are defined by

$$\psi = (u_e \nu s_1)^{\frac{1}{2}} h_2 f(x,z,\eta) \tag{7a}$$

$$\phi = (u_e \nu s_1)^{\frac{1}{2}} h_1 (w_e/u_e) g(x,z,\eta) \tag{7b}$$

Here s_1, which denotes the arc length along the x coordinate, is defined by

$$s_1 = \int_0^x h_1 dx \tag{8}$$

The parameters K_1 and K_2 in Eq. (2) are defined by

$$K_1 = -\frac{1}{h_1 h_2}\frac{dh_1}{dz} \qquad \text{and} \qquad K_2 = -\frac{1}{h_1 h_2}\frac{dh_2}{dx}$$

With the concept of eddy viscosity and with the previous transformed variables, it can be shown that the system of Eqs. (1) through (4) can be written as

x-Momentum Equation

$$(bf'')' + P_1 ff'' + P_2[1 - (f')^2] + P_5[1 - f'g']$$

$$+ P_6 f''g + P_8[1 - (g')^2]$$

$$= xP_{10}\left[f'\frac{\partial f'}{\partial x} - f''\frac{\partial f}{\partial x} + P_7\left(g'\frac{\partial f}{\partial z} - f''\frac{\partial g}{\partial z}\right)\right] \tag{9}$$

z-Momentum Equation

$$(bg'') + P_1 fg'' + P_4(1 - f'g') + P_3[1 - (g')^2]$$

$$+ P_6 gg'' + P_9[1 - (f')^2]$$

$$= xP_{10}\left[f'\frac{\partial g'}{\partial x} - g''\frac{\partial f}{\partial x} + P_7\left(g'\frac{\partial g'}{\partial z} - g''\frac{\partial g}{\partial z}\right)\right] \tag{10}$$

$$\eta = 0 \qquad f = g = f' = g' = 0 \tag{11a}$$

$$\eta = \eta_\infty \qquad f' = g' = 1 \tag{11b}$$

Here the primes denote differentiation with respect to , and

$$b = 1+\varepsilon^{+} \qquad \varepsilon^{+} = \varepsilon/\nu \qquad f' = u/u_e \qquad g' = w/w_e \tag{12a}$$

The coefficients P_1 to P_{10} are functions of u_e, w_e, h_1, h_2, K_1, and K_2 and are given by the following formulas:

$$P_1 = (M+1)/2 - s_1 K_2 \qquad P_2 = M \qquad P_3 = R$$

$$P_4 = \left(\frac{u_e}{w_e}\right) Q - s_1 K_2 \qquad P_5 = \frac{w_e}{u_e}\,(N - s_1 K_1)$$

$$P_6 = R + \frac{w_e}{2u_e}\left(\frac{1}{h_1}\frac{\partial s_1}{\partial z} - N\right) - \left(\frac{w_e}{u_e}\right) s_1 K_1$$

$$P_7 = \frac{h_1}{h_2}\frac{w_e}{u_e} \qquad P_8 = \left(\frac{w_e}{u_e}\right)^2 s_1 K_2$$

$$P_9 = \left(\frac{u_e}{w_e}\right) s_1 K_1 \qquad P_{10} = \frac{s_1}{x h_1} \tag{12b}$$

$$M = \frac{s_1}{u_e h_1}\frac{\partial u_e}{\partial x} \qquad N = \frac{s_1}{u_e h_2}\frac{\partial u_e}{\partial z}$$

$$Q = \frac{s_1}{u_e h_1}\frac{\partial w_e}{\partial x} \qquad R = \frac{s_1}{u_e h_2}\frac{\partial w_e}{\partial z}$$

In order to solve Eqs. (9) through (11), initial conditions are required at a starting plane. In the case of the boundary-layer problem,

the initial conditions at x = 0 and z = 0 planes are obtained by solving the limiting form of Eqs. (9) and (10). For a wall jet, initial velocity profiles are prescribed at some downstream x plane and along the z = 0 plane, attachment line equations are solved. The attachment line equations are obtained by differentiating the z-momentum equation with respect to z and setting

$$w = \frac{\partial p}{\partial z} = \frac{\partial u}{\partial z} = \frac{\partial v}{\partial z} = \frac{\partial^2 w}{\partial z^2} = 0$$

The resulting attachment line equations valid at the z = 0 plane are

$$(bf'')' + P_1 ff'' + P_2[1 - (f')^2] + P_3 gf'' = xP_{10}\left[f' \frac{\partial f'}{\partial x} - f'' \frac{\partial f}{\partial x}\right] \qquad (13)$$

$$(bg'')' + P_1 fg'' + P_4(1 - f'g') + P_3[1 - (g')^2]$$

$$+ P_3 gg'' = xP_{10}\left[f' \frac{\partial g'}{\partial x} - g'' \frac{\partial f}{\partial x}\right] \qquad (14)$$

Here, g' is defined as w_z/w_{e_z}

Eddy-Viscosity Model

Eqs. (2) and (3) contain Reynolds shear stress terms $-\overline{u'v'}$ and $-\overline{v'w'}$. In order to satisfy the closure assumptions for these shear stress terms, we use the eddy viscosity concept and define

$$-\overline{u'v'} = \varepsilon u_y = \bar{\varepsilon}\left[1 - \frac{C_1 u \kappa_2}{1 + \kappa_2 y} \frac{1}{u_y}\right] u_y$$

$$-\overline{w'v'} = \varepsilon w_y = \bar{\varepsilon}\left[1 - \frac{C_2 w \kappa_1}{1 + \kappa_1 y} \frac{1}{w_y}\right] w_y \qquad (15)$$

The second term inside the bracket in Eq. (15) is due to curvature where κ_1 and κ_2 denote the radius of curvature of z = const. and x = const. lines. The quantity $\bar{\varepsilon}$ is assumed to be same in both the x and z directions and is represented by a two-layer model. Referring to Fig. 2, the structure of these layers is as follows:

First Layer

$$\left.\begin{aligned} &\bar{\varepsilon} = (0.435\ y)^2 \sqrt{u_y^2 + w_y^2} \qquad 0 \leqslant y \leqslant y^* \\ &\text{Second Layer} \\ &\bar{\varepsilon} = (0.125\ y_1)^2 \sqrt{u_y^2 + w_y^2} \qquad y \geqslant y^* \end{aligned}\right\} \tag{16}$$

where at $y = y_1$,

$$\frac{\left|\sqrt{u_e^2 + w_e^2} - \sqrt{u^2 + w^2}\right|}{\sqrt{u_e^2 + w_e^2}} \cong 0.01$$

and y* is obtained by imposing continuity in $\bar{\varepsilon}$ at $y = y^*$. This yields $y^* = \frac{0.125}{0.435}\, y_1$. C_1 and C_2 appearing in Eq. (15) can be assigned values between one and three.

Finite Difference Equations

First, reduce the system (9)-(10) to the first order system

$$f' = u \tag{17}$$

$$u' = v \tag{18}$$

$$g' = w \tag{19}$$

$$w' = t \tag{20}$$

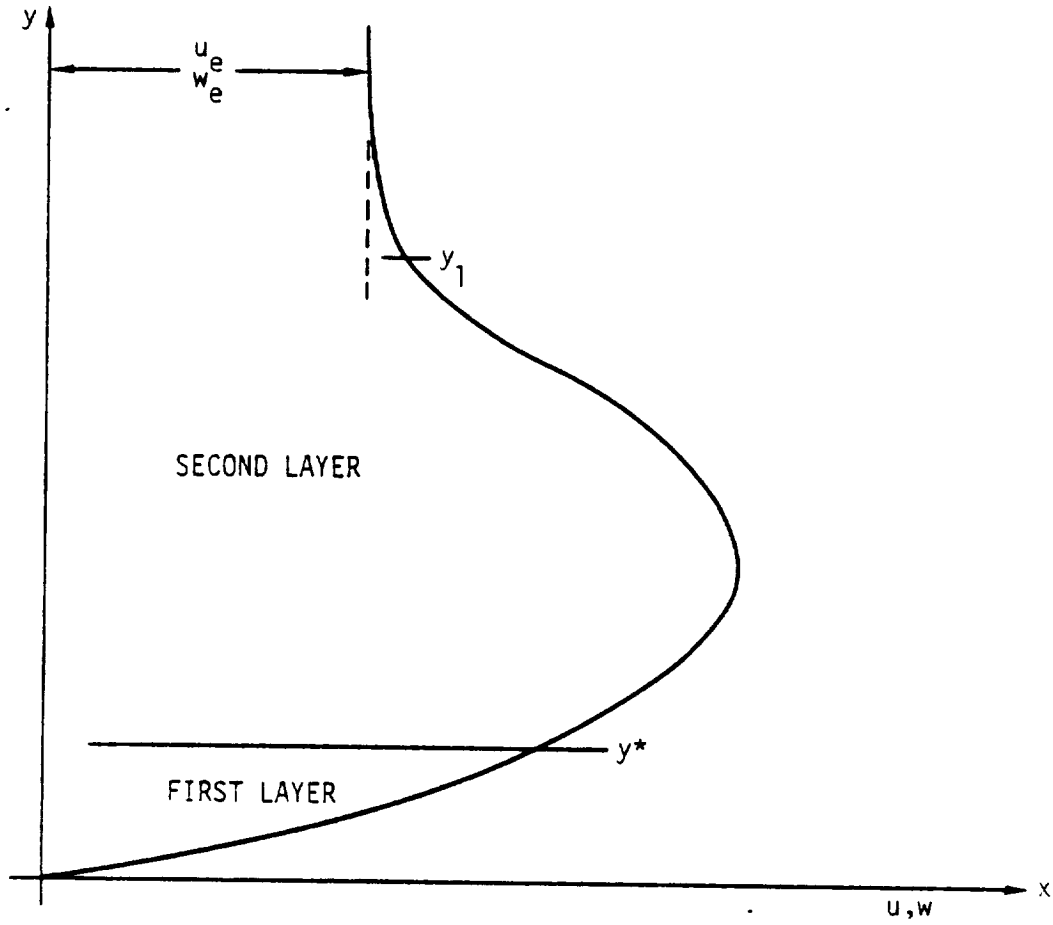

Figure 2.- Two-layer eddy viscosity model.

$$(bv)' + P_1 fv + P_2(1 - u^2) + P_5[1 - uw]$$

$$+ P_6 vg + P_8[1 - w^2] = xP_{10}\left[u\frac{\partial u}{\partial x} - v\frac{\partial f}{\partial x} + P_7\left(w\frac{\partial u}{\partial z} - v\frac{\partial g}{\partial z}\right)\right] \quad (21)$$

$$(bt)' + P_1 ft + P_4(1 - uw) + P_3(1 - w^2) + P_6 gt$$

$$+ P_9(1 - u^2) = xP_{10}\left[u\frac{\partial w}{\partial x} - t\frac{\partial f}{\partial x} + P_7\left(w\frac{\partial w}{\partial z} - t\frac{\partial g}{\partial z}\right)\right] \quad (22)$$

Let

$$x_0 = \text{constant} \qquad x_n = x_{n-1} + k_n \qquad n = 1,2,\ldots,N$$

$$z_0 = 0 \qquad z_i = z_{i-1} + r_i \qquad i = 1,2,\ldots,I$$

$$\eta_0 = 0 \qquad \eta_j = \eta_{j-1} + h_j \qquad j = 1,2,\ldots,J$$

Then, using the box method, we have

$$\frac{f_j^{n,i} - f_{n-1}^{n,i}}{h_j} = u_{j-\frac{1}{2}}^{n,i} \quad (23)$$

$$\frac{u_j^{n,i} - u_{j-1}^{n,i}}{h_j} = v_{j-\frac{1}{2}}^{n,i} \quad (24)$$

$$\frac{g_j^{n,i} - g_{j-1}^{n,i}}{h_j} = w_{j-\frac{1}{2}}^{n,i} \quad (25)$$

$$\frac{w_j^{n,i} - w_{j-1}^{n,i}}{h_j} = t_{j-\frac{1}{2}}^{n,i} \quad (26)$$

We use the notation

$$\bar{P} = P^{n-\frac{1}{2},\,i-\frac{1}{2}}_{j-\frac{1}{2}} \equiv P^{n-\frac{1}{2}}_{i-\frac{1}{2}}$$

and

$$\bar{v}_j = \frac{1}{4}\left(v^{n,i}_j + v^{n,i-1}_j + v^{n-1,i-1}_j + v^{n-1,i}_j\right)$$

$$\bar{u}_i = \frac{1}{2}\left(u^{n,i}_{j-\frac{1}{2}} + u^{n,i-1}_{j-\frac{1}{2}}\right)$$

$$\bar{u}_n = \frac{1}{2}\left(u^{n,i}_{j-\frac{1}{2}} + u^{n-1,i}_{j-\frac{1}{2}}\right)$$

Equation (21) becomes, with the box centered at $(x_{n-\frac{1}{2}}, z_{i-\frac{1}{2}}, \eta_{j-\frac{1}{2}})$

$$\begin{aligned}
&(\bar{b}_j\bar{v}_j - \bar{b}_{j-1}\bar{v}_{j-1})/h_j \\
&\quad = -\bar{P}_1(\overline{fv})_{j-\frac{1}{2}} - \bar{P}_2(1 - \bar{u}^2_{j-\frac{1}{2}}) - \bar{P}_5(1 - \bar{u}_{j-\frac{1}{2}}\bar{w}_{j-\frac{1}{2}}) \\
&\qquad - \bar{P}_6(\overline{vg})_{j-\frac{1}{2}} - \bar{P}_8(1 - \bar{w}^2_{j-\frac{1}{2}}) \\
&\qquad + x_{n-\frac{1}{2}}\bar{P}_{10}\left\{u_{j-\frac{1}{2}}\frac{(\bar{u}_n - \bar{u}_{n-1})}{k_n} - \bar{v}_{j-\frac{1}{2}}\frac{(\bar{f}_n - \bar{f}_{n-1})}{k_n}\right. \\
&\qquad \left. + \bar{P}_7\left[\bar{w}_{j-\frac{1}{2}}\frac{(\bar{u}_i - \bar{u}_{i-1})}{r_i} - \bar{v}_{j-\frac{1}{2}}\frac{(\bar{g}_i - \bar{g}_{i-1})}{r_i}\right]\right\}
\end{aligned} \tag{27}$$

Equation (22) and the attachment line equations (13)-(14) are discretized similarly. Details of the procedure are given in Ref. 4.

The solution procedures involves the following steps:

(1) Solve the attachment line equations (13)-(14) with boundary conditions (11) at $x = x_1$ and $z = 0$ assuming initial conditions on $x = x_0$.

(2) March in the z-direction along the plane $x = x_1$ and solve equations (17)-(22) with boundary conditions (11) for the unknowns (f,u,v,g,w,t).

(3) Repeat steps (1) and (2) for the next x-plane, $x = x_2$, and so on.

The most efficient way to solve the finite difference equations is to use a pseudo-Newton's relaxation scheme. These equations may be written as a system of nonlinear algebraic equations by writing

$$\underset{\sim}{\Phi}(\underset{\sim}{u}) = 0$$

where

$$\underset{\sim}{u} = (f_j^{n,i},\ u_j^{n,i},\ v_j^{n,i},\ g_j^{n,i},\ w_j^{n,i},\ t_j^{n,i})_{j=0}$$

Then, the relaxed Newton's method becomes

$$\frac{\partial \underset{\sim}{\Phi}^{(\nu-1)}}{\partial \underset{\sim}{u}} \delta \underset{\sim}{u}^{(\nu-1)} = - \underset{\sim}{\Phi}\left(\underset{\sim}{u}^{(\nu-1)}\right) \tag{28a}$$

$$\underset{\sim}{u}^{(\nu)} = \underset{\sim}{u}^{(\nu-1)} + \omega \delta \underset{\sim}{u}^{(\nu-1)} \tag{28b}$$

for $\nu = 1,2,\ldots$

The method is said to have converged when

$$\| \delta \underset{\sim}{u}^{(\nu-1)} \|_{\infty} \leqslant \varepsilon \text{ (a prescribed error tolerance)}$$

We call Eq. (28) a pseudo-Newton's method because we linearize the b terms in equations (21) and (28) by evaluating them at $\nu-2$ before computing the Jacobian matrix, $\partial \underset{\sim}{\Phi} / \partial \underset{\sim}{u}$. Consequently, this algorithm will not be quite quadratically convergent. We, therefore, employ relaxation ($\omega \neq 1$) to accelerate it. Remarkably, underrelaxation ($\omega < 1$) works very well, while overrelaxation ($\omega > 1$) diverges. Values of w of 0.5, 0.6, 0.7, 0.9, and 0.9 all give good results with $\omega = 0.7$ slightly the overall best for some of our computational experiments.

An important feature of Keller's box method is that the Jacobian matrix can be put into block tridiagonal form and very efficient elimination schemes can be employed for solving equation (28a).

Minor Difficulties with the Numerical Algorithm

When starting at $x = x_0 \neq 0$ with supplied velocity profiles, unnatural oscillations developed in the solution. This difficulty was eliminated completely by employing the following "trick." The first 10 mesh points in the x-direction were set at $k_n = 10^{-4}$. For the first five planes in the x-direction and all points in the z-direction in these planes, an average value was used for past points, i.e.,

$$f_j^{n-1,i} = 0.5\left(f_j^{n-1,i} + f_j^{n-2,i}\right) \quad , \quad f_j^{n,i-1} = 0.5\left(f_j^{n,i-1} + f_j^{n,i-2}\right)$$

and

$$f_j^{n-1,i-1} = 0.5\left(f_j^{n-1,i-1} + f_j^{n-2,i-1}\right)$$

Beginning with the sixth x-plane, the averaging was eliminated (the standard algorithm was employed). At the eleventh x-plane a geometric mesh-stretching algorithm of the following form was used:

$$k_n = 1.2k_{n-1} \quad , \quad n = 11,12,13,...$$

No such stretching has been employed in the z-direction, but in the future it may also be required for rapidly changing profiles. It should be noted that our averaging algorithm was required in both the x and z directions to remove all oscillations.

A mesh refinement algorithm is used which adds or deletes points depending on the relative local variation in the truncation error of the difference equations. Roughly 80 grid points in the η-direction and 11 grid points in the z-direction are employed.

Results

Computations were performed on the Berkeley CDC 7600 machine. A typical calculation required about 6 minutes of CPU time. Fig. 3 indicates the external and initial velocity distributions which have been used as a basis for our calculations. The parameter θ was introduced as shown to vary the initial cross flow while keeping the total velocity constant as a rough simulation of a fixed supply of engine mass flow. The velocity profile was selected to have a characteristic fully developed character associated with turbulent wall jet flows. Future aspects of this effort will consider the "eating up" of the potential core which is assumed to occur upstream of the initial station of this analysis. The parameters C_2 and C_3 were chosen to provide slope and value continuity of the profile at $y = y_{max}$. For $y \geq y_{max}$ the profile has a half Gaussian character associated with a free jet. For $y \leq y_{max}$ the profile has a boundary-layer character. In the examples, the u and w initial profiles were assumed to be identical. Moreover, the θ distribution was selected to be

EXTERNAL VELOCITY

$$u_e = U_0 x^{-n} \cos\theta$$

$$w_e = U_0 x^{-n} \sin\theta$$

$$\theta = C z (z_{tip} - z) \frac{\pi}{2}$$

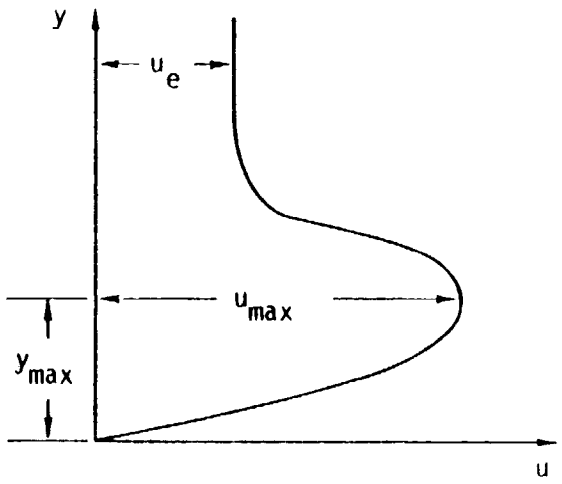

INITIAL PROFILE

$$\frac{u}{u_e} = \begin{cases} C_2 (e^{-y} - 1) + C_3 y & y \leq y_{max} \\ 1 + \left(\frac{u_{max}}{u_e} - 1\right) e^{-0.1(y - y_{max})^2} & y \geq y_{max} \end{cases}$$

$$\frac{w}{w_e} = \text{SAME AS } \frac{u}{u_e} \text{ PROFILE}$$

- SMALL CROSS FLOW IS ACHIEVED BY SETTING C IN θ VERY SMALL (10^{-15})

Figure 3.- Initial and boundary conditions.

qualitatively similar to that observed by rake surveys on the XFV-12A. The zero cross flow case was achieved by setting C to 10^{-15}.

Figure 4 demonstrates decay of the peak velocity with the standardized distributions of Fig. 3, with and without cross flow. It is evident from the figure that cross flow has a dramatic effect on enhancing the decay of the maximum velocity. In the calculations, the exponent n in the external velocities is assumed as ½, roughly in accord with a value obtained from a two-dimensional line sink simulating inflow originally proposed by G.I. Taylor.[5] In a more realistic model, these external velocity distributions should be corrected for three-dimensionality and elliptic interaction with the wall jet. A calculation of this type would be a more accurate representation than the present approach of planform and surface curvature effects. In this connection, we recognize that that means of simulating taper, sweepback, and spanwise pressure gradients in the present analysis is solely through cross flow adjustment.

The three-dimensional inviscid potential ϕ can be characterized by a surface sink distribution of the form (see Fig. 5)

$$\phi(x,y,z) = \frac{1}{4\pi} \iint_S \frac{\sigma(\xi,\zeta)d\xi d\zeta}{\sqrt{(x-\xi)^2 + y^2 + (z-\zeta)^2}} \tag{29}$$

where S the area of integration refers to the total jet area on and off the wing. The quantity σ is the sink strength obtained by matching with an "outer limit" of the second order solution for the velocity normal to the body appearing in the viscous inner wall jet solution. The quantity σ for two-dimensional boundary layers is analogous to the streamwise gradient of the displacement thickness $\delta'(x)$. To include lifting surface effects, a surface doublet or vortex distribution should be added to (29). The local vortex strength can also be determined by matching.

The inflow velocity related to the sink intensity σ in (29) is in turn a function of the entrainment. This quantity is also significant

$$u_e = u_o x^{-1/2} \cos\theta,\ w_e = u_o x^{-1/2} \sin\theta,\ \theta = \frac{\pi}{2} z(z_{tip} - z)$$

STANDARD INITIAL PROFILE ($z = z_1$)

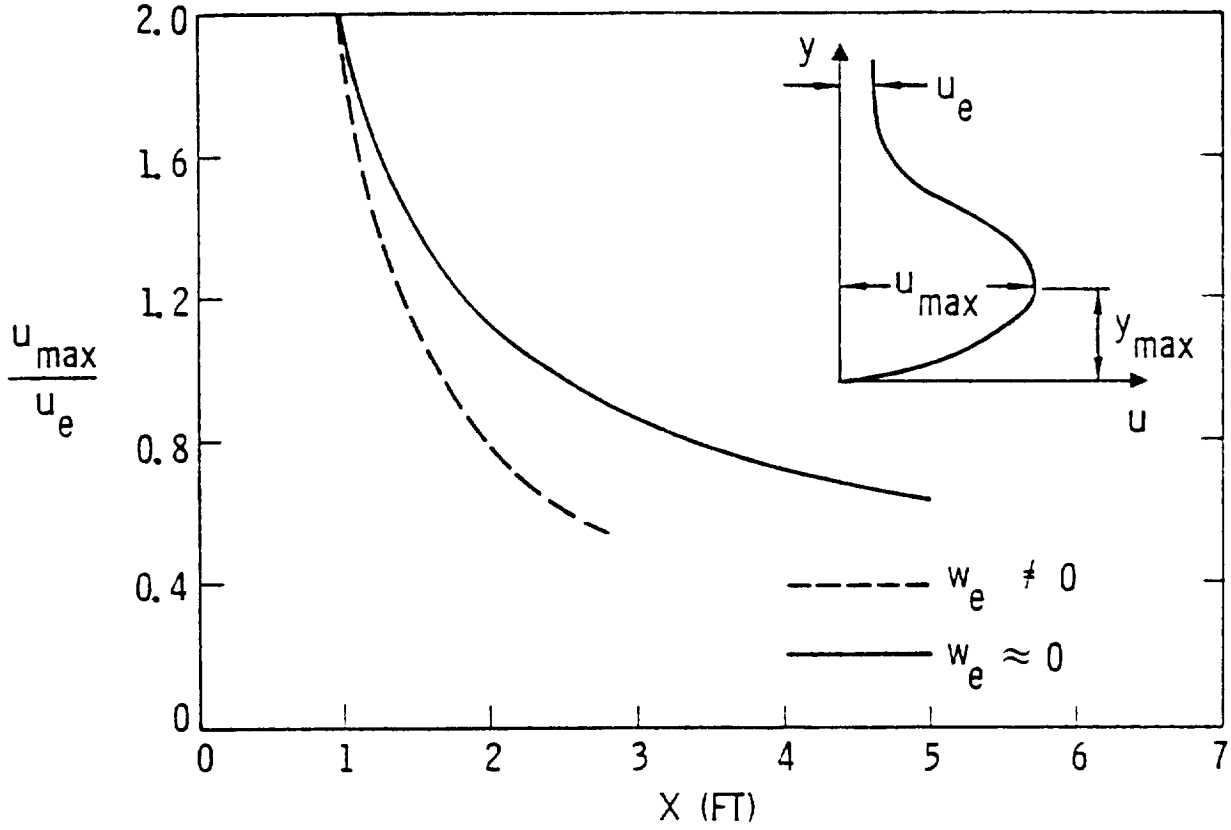

Figure 4.- Effect of cross flow on jet growth.

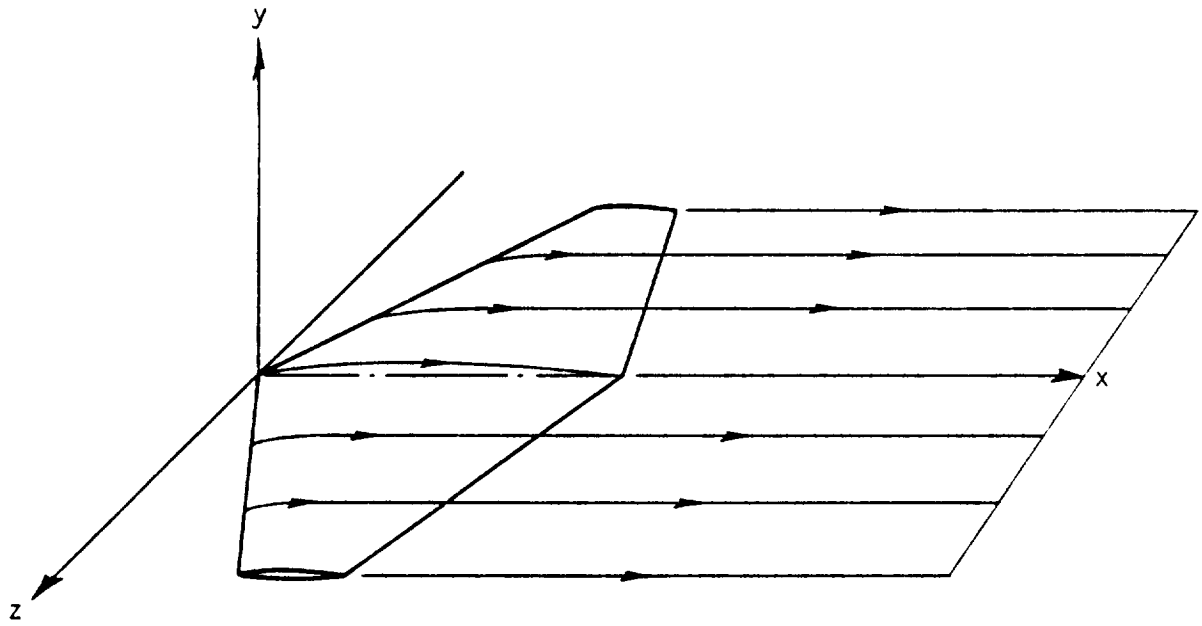

Figure 5.- Tapered thrust augmented wing (TAW).

from the standpoint of the tradeoff between skin friction, BLC, and rapid acceleration of the secondary in compact three-dimensional thrust augmenting ejectors such as those employed on the XFV-12A and upper surface blowing.

In Fig. 6, the comparison between cross flow and the absence of it gives the indicated entrainment variations with streamwise distance. In spite of the appreciable increase in decay of the maximum value of u shown in Fig. 4, and resultant shear stress in Fig. 7, only a slight difference in entrainment quantity and rate is shown in Fig. 6. The difference in maximum velocities which are similar for w, the spanwise component, are presumably related to the enhanced dissipation associated with cross flow and that implied by the eddy viscosity model. The lack of a corresponding decrease in entrainment rate may be due to nonlinear compensating effects built into the turbulence model and cannot be readily explained on an intuitive basis at this time. In this connection, other calculations will be performed for which the streamwise component of the initial velocity is held fixed rather than its overall magnitude on introduction of cross flow. It should be noted that the expression for entrainment Q given in Fig. 6 assumes that w at the tip $z = z_{tip} = 0$. If this is not the case, an additional term must be added to this relation.

Associated with the previous results, Fig. 8 shows the effect of cross flow on jet spreading rate related to y_{max}. As previously, only small differences are indicated for the cases considered. In Fig. 9, however, an important upstream movement of the separation line is indicated with the introduction in cross flow. This result is significant with respect to penalties associated with taper and sweep in three-dimensional ejector diffusors.

In Fig. 10, another important consequence of cross flow is examined in connection with the surface streamline pattern. In the figure, two cases are compared involving differing amounts of cross flow. Significant enhancement in downstream streamtube contraction is obvious with increase in cross flow. This contraction could presumably lead to end wall separation of the type observed on the XFV-12A.

$$u_e = u_o x^{-1/2} \cos\theta, \quad w_e = u_o x^{-1/2} \sin\theta, \quad \theta = C\frac{\pi}{2} z(z_{tip} - z)$$

$$Q = \int_0^{\infty} \int_0^{z_{tip}} u\,dy\,dz$$

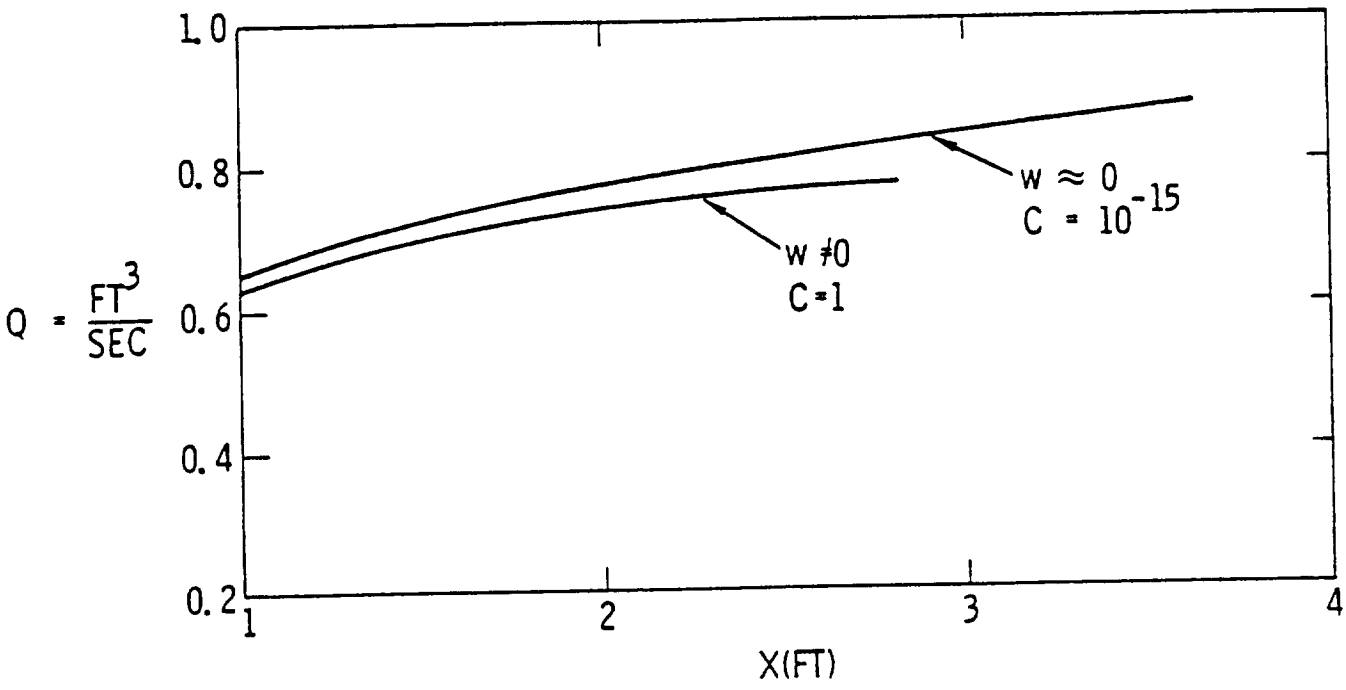

Figure 6.- Effect of cross flow on entrainment.

$$u_e = u_0 x^{-1/2} \cos\theta, \quad w_e = u_0 x^{-1/2} \sin\theta, \quad \theta = C\frac{\pi}{2} z (z_{tip} - z)$$

STANDARD INITIAL PROFILE ($z = z_1$)

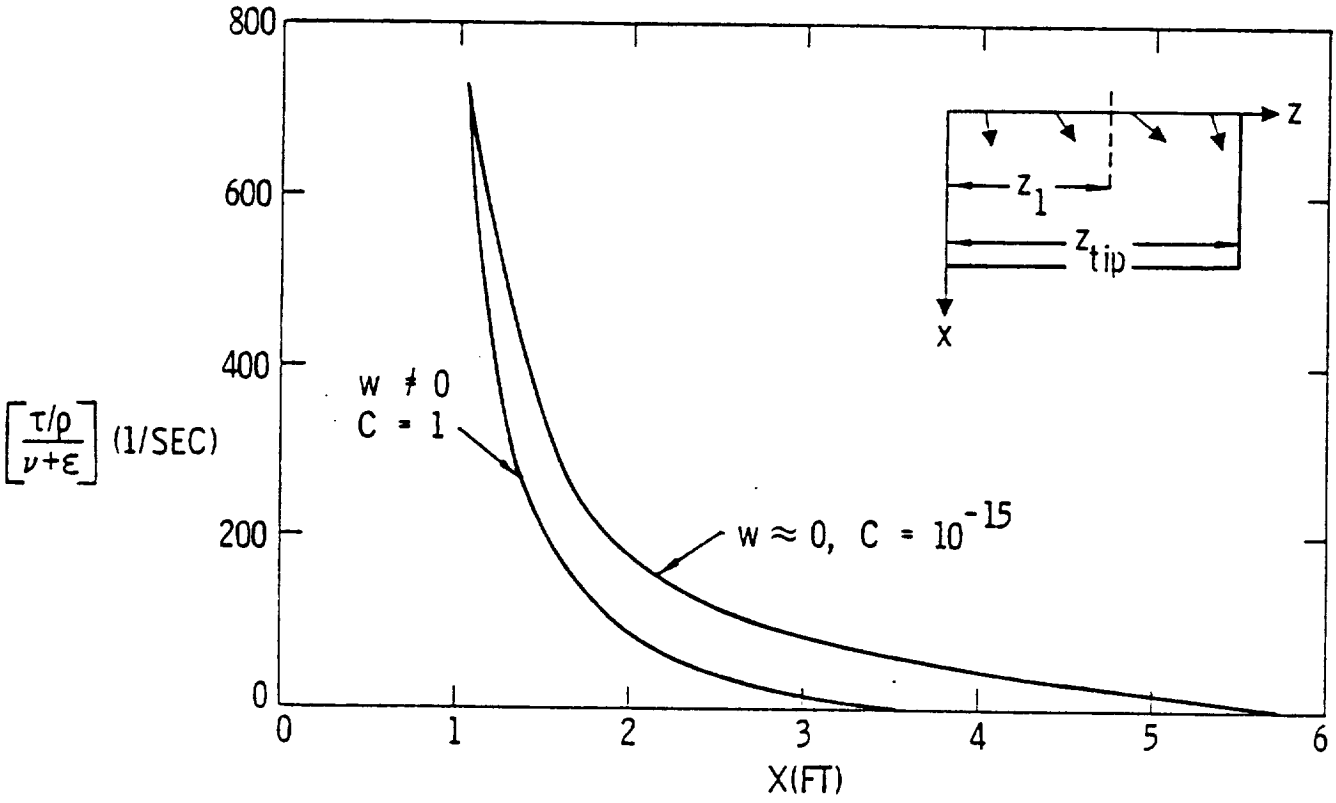

Figure 7.- Effect of cross flow on reduced shear stress.

$$u_e = u_o x^{-1/2} \cos\theta, \quad w_e = u_o x^{-1/2} \sin\theta, \quad \theta = C\frac{\pi}{2} z (z_{tip} - z)$$

STANDARD INITIAL PROFILE PLOTTED AT MIDSPAN

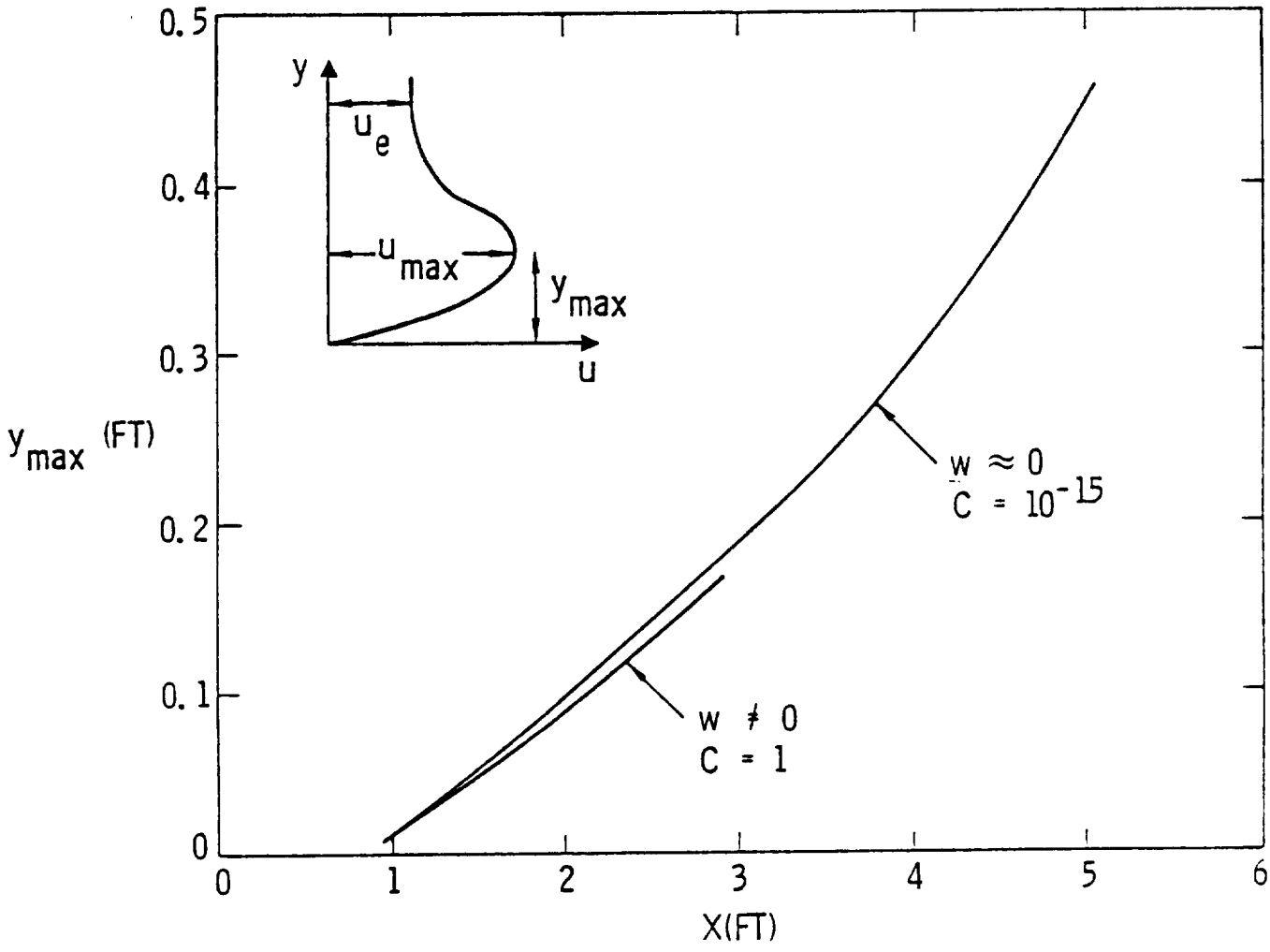

Figure 8.- Effect of cross flow on jet spreading.

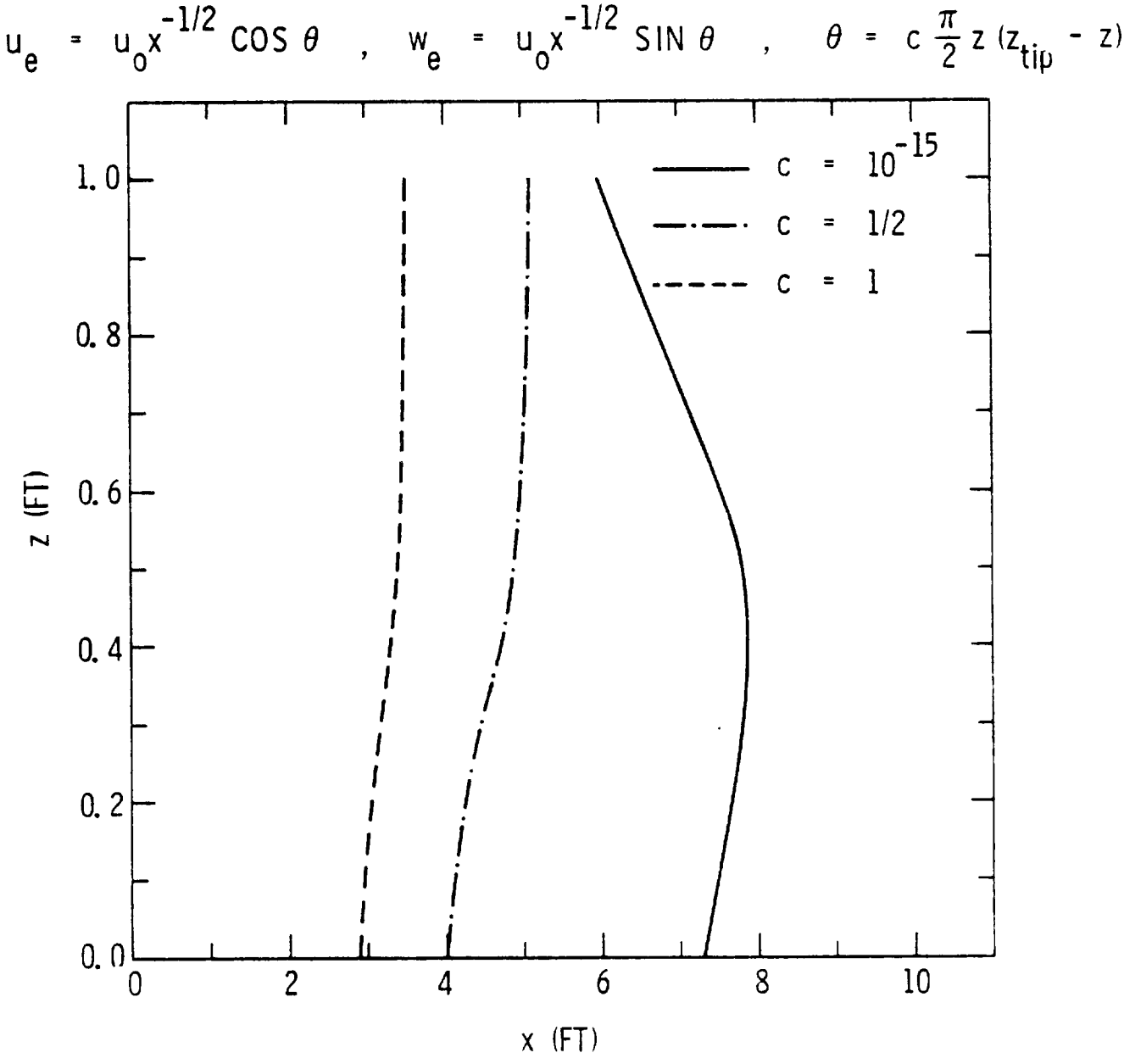

Figure 9.- Effect of cross flow on the locus of nominal separation.

$$u_e = u_0 x^{-1/2} \cos\theta \quad , \quad w_e = u_0 x^{-1/2} \sin\theta$$

——— $\theta = \frac{c\pi}{2} z (z_{tip} - z)$

- - - - - $\theta/2$

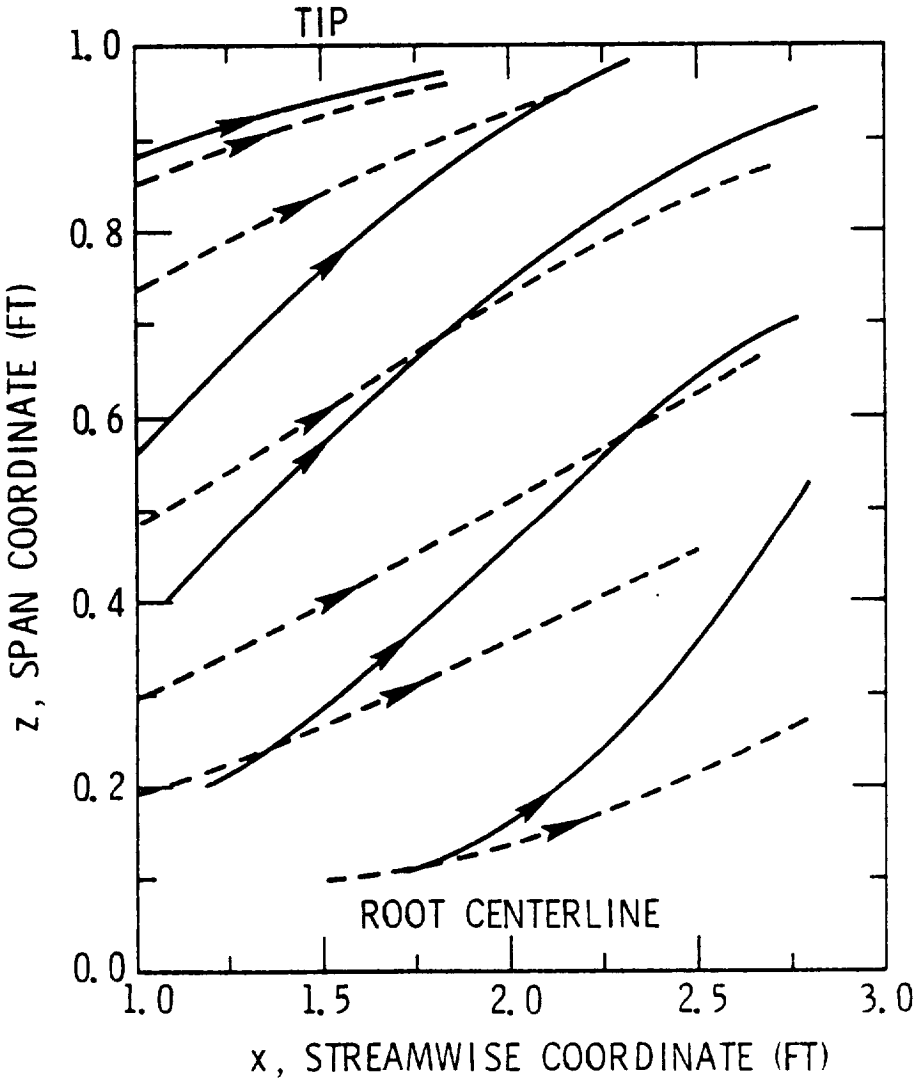

Figure 10.- Cross flow effect on jet "shrink" and "end-wall pullaway."

Conclusions

A class of cases were investigated roughly possessing initial flow angularity and adverse pressure gradients prototypic of those on the XFV-12A. Results obtained from the computational model indicate that if the initial total velocity is kept fixed then the introduction of the cross flow enhances the decay rate of the peak of the streamwise velocity component. In addition, the entrainment quantity and its rate decrease with increased cross flow. The implication of this phenomenon with respect to taper effect on boundary layer control (BLC) of the XFV-12A Coandas is not as significant as a "jet shrink" which has also been indicated in our approximate three-dimensional model. This contraction has been postulated as a mechanism promoting end-wall separation. To our knowledge, our model is the first to quantify such trends. Finally, the effect on the prescribed external adverse pressure gradient in the presence and absence of cross flow has also been examined. From the limited results, the spanwise separation line moves progressively further upstream with increasing cross flow.

References

1. Keller, H.B. and Cebeci, T., "Accurate Numerical Methods for Boundary Layers, I. Two-Dimensional Laminar Flows," Proceedings of the Second International Conference on Numerical Methods in Fluid Dynamics, Lecture Notes in Physics, Springer-Verlag, New York, Vol. 8, 1971.

2. Keller, H.B. and Cebeci, T., "Accurate Numerical Methods for Boundary Layers, II. Two-Dimensional Turbulent Flows," AIAA Journal, Vol. 10, September 1972, pp. 1197-1200.

3. Cebeci, T., "Calculation of Three Dimensional Boundary Layers, II. Three Dimensional Flows in Cartesian Coordinates," AIAA J., Vol. 13, No. 8, p. 1056, 1975.

4. Murphy, W.D., Shankar, V., and Malmuth, N.D., "Three Dimensional Wall Jets," Quarterly Progress Report No. 2, NADC Contract No. N62269-77-C-0412.

5. Taylor, G.I., J. of Aero. Sci., 25, 7, pp. 464-5 (1958).